Available online at www.sciencedirect.com
ScienceDirect
Thermochimica Acta 462 (2007) 15–24
thermochimica acta
www.elsevier.com/locate/tca

Enthalpy-based determination of crystalline, mobile amorphous and rigid amorphous fractions in semicrystalline polymers Poly(ethylene terephthalate)

Maria Cristina Righetti [a,*], Elpidio Tombari [a], Marco Angiuli [a], Maria Laura Di Lorenzo [b]

[a] *Istituto per i Processi Chimico-Fisici (Consiglio Nazionale delle Ricerche), Area della Ricerca, Via G. Moruzzi, 1, 56124 Pisa, Italy*
[b] *Istituto di Chimica e Tecnologia dei Polimeri (Consiglio Nazionale delle Ricerche), c/o Comprensorio Olivetti, Via Campi Flegrei, 34, 80078 Pozzuoli (NA), Italy*

Received 12 April 2007; received in revised form 13 June 2007; accepted 16 June 2007
Available online 20 June 2007

Abstract

A new method to simultaneously monitor the development of crystalline, mobile amorphous and rigid amorphous fractions during cooling from the melt in semicrystalline polymers is here presented. The method, which allows the determination of the temperature evolution of the three nanophases, is the development of a previous enthalpy-based procedure founded on a two-phase description of the semicrystalline polymers, with only one crystalline phase and one amorphous phase accounted for. The proposed method has been applied to determine the development of the nanophase structure in poly(ethylene terephthalate) (PET) upon cooling from the melt. In addition the temperature-dependent enthalpy of the rigid amorphous phase has been calculated. For the cooling rates investigated, it was found that the rigid amorphous fraction starts to vitrify when the crystallization process is almost finished and continues further on cooling to the glass transition of the bulk amorphous phase. A possible connection between secondary crystallization and initial vitrification of the rigid amorphous phase has been hypothesized for PET.

Keywords: Three-phase system; Crystalline fraction; Mobile amorphous fraction; Rigid amorphous fraction; Enthalpy

1. Introduction

Semicrystalline polymers have a metastable nanophase structure, where the various nanophases can be crystal, liquid, glass, or mesophase [1–4]. This multi-level structure is determined by a competition among self-organization, crystallization, and vitrification and is established during material processing. Early investigations of semicrystalline polymers based their description on a two-phase model, where the two phases, an amorphous and a crystalline one, may have nanometer dimensions in one or more directions. Recently, more detailed analyses revealed that an intermediate nanophase must be present at the interface between the crystals and the surrounding melt [4,5]. The intermediate phase is non-crystalline, and arises from the continuation of the partially crystallized macromolecules across the phase boundaries, as the polymer molecules are much longer than the crystal nanophases. This phase, that includes portions of macromolecules whose mobility is hindered by the near crystalline structures, is generally named "rigid amorphous fraction" (RAF), being its mobility lower than that of the unstrained amorphous phase, which is usually addressed as "mobile amorphous fraction" (MAF). The temperature at which RAF mobilizes is often located between the T_g of the unstrained amorphous phase and the melting temperature, but this is not a general rule. Some semicrystalline polymers may have no RAF, or may have a RAF which mobilizes in correspondence of the melting, or even above the melting point [5].

The amount of rigid amorphous fraction in a semicrystalline polymer is generally quantified by difference, after determination of the crystalline and mobile amorphous phase contents, being:

$$w_C + w_A + w_{RA} = 1 \quad (1)$$

where w_C, w_A, and w_{RA} are the crystalline, mobile amorphous, and rigid amorphous weight fractions, respectively.

* Corresponding author. Tel.: +39 050 3152068; fax: +39 050 3152230.
E-mail address: righetti@ipcf.cnr.it (M.C. Righetti).

0040-6031/$ – see front matter © 2007 Elsevier B.V. All rights reserved.
doi:10.1016/j.tca.2007.06.003

Up to now some studies have been performed on the kinetics of formation of the RAF and its devitrification [6–10]. For some polymers like poly(3-hydroxybutyrate), polycarbonate and isotactic polystyrene, parallel development of the RAF with crystallinity has been detected, whereas only partial formation of RAF during crystallization has been evidenced for syndiotactic polypropylene and poly(ethylene terephthalate) at some particular crystallization temperatures [7–10]. In these studies the simultaneous development of the crystal phase and the rigid amorphous fraction has been monitored at a single temperature.

It has been also demonstrated that generally devitrification of the RAF occurs simultaneously with melting [6–8,11] even if there are some exceptions. For poly(oxy-2,6-dimethyl-1,4-phenylene), for example, it has been shown that the RAF glass transition temperature, higher than the melting temperature, can delay fusion on heating until enough mobility is present at the crystal surface [12].

The proof that formation and loss of rigid-amorphous fraction and crystals go parallel is of great importance for the understanding of polymer physical properties [13,14]. It would be very advantageous to develop a method able to determine quantitatively the interrelation between crystalline, rigid and mobile amorphous phase contents not only at a given temperature, but in a wide temperature range, also during heating and cooling at controlled rate.

An interesting procedure, based on a model that needs some morphological assumptions about the structure of a semicrystalline polymer, was introduced few years ago with the aim of determining the temperature dependence of crystalline, rigid-amorphous and mobile amorphous fractions during fusion [6]. The approach, that was proposed for samples of low-density and high density polyethylene, involves an adjustable parameter, the thickness of the RAF layer, assumed temperature independent, and other quantities that, connected to the thermodynamics of crystallization, are not easily accessible for all the polymers.

A new and simpler method to simultaneously monitor the development of crystalline, mobile amorphous and rigid amorphous fractions during cooling from the melt in semicrystalline polymers is proposed in the present study. The method is the development of a previous enthalpy-based procedure founded on a two-phase description of semicrystalline polymers, with only the crystalline and the mobile amorphous phase accounted for [15,16].

According to the two-phase model, the experimental enthalpy of semicrystalline polymers, $h(T)$, can be expressed as [15,16]:

$$h(T) = w_C(T)h_C(T) + w_A(T)h_A(T) \quad (2)$$

where $w_C(T)$ and $w_A(T)$ are the crystal and mobile amorphous weight fractions, with $[w_C(T) + w_A(T)] = 1$, and $h_C(T)$ and $h_A(T)$ the temperature-dependent enthalpies of the crystalline and mobile amorphous polymer respectively. Opportune elaboration of Eq. (2) brings to:

$$w_C(T) = \frac{h_A(T) - h(T)}{h_A(T) - h_C(T)} \quad (3)$$

according to which $w_C(T)$ can be calculated for a two-phase model, being $[h_A(T) - h(T)]$ easily obtained through a simple integration of the experimental heat capacity data [15,16] and the difference $[h_A(T) - h_C(T)]$ available from the ATHAS Data Bank for more than 200 different polymers [17].

The temperature derivative of Eq. (2) defines the specific heat capacity:

$$c_p(T) = w_C(T)c_{p,C}(T) + w_A(T)c_{p,A}(T) - [h_A(T) - h_C(T)] \times \frac{dw_C(T)}{dT} \quad (4)$$

where $c_p(T)$ is the measured specific heat capacity, $c_{p,C}(T)$ and $c_{p,A}(T)$ the thermodynamic values of the crystalline and mobile amorphous specific heat capacities and $[h_A(T) - h_C(T)]$ the heat of fusion, all tabulated in the ATHAS Data Bank [17].

Since it was proposed, very little improvement of the above detailed enthalpy-based method has been published, the only exception being its adaptation to multi-component polymer systems [18]. In this article we propose a reworking and development of Eqs. (2)–(4) applied to a three-phase system, in order to determine the crystalline, mobile amorphous and rigid amorphous phase contents of a semicrystalline polymer during non-isothermal crystallization.

Poly(ethylene terephthalate) (PET) was chosen as a model polymer to test the method, since PET can form relatively large amount of RAF, the different contents of the three nanophases being easily modulated in dependence on crystallization conditions [5].

2. Experimental

Poly(ethylene terephthalate) of molar mass $M_w = 21\,400$ g mol^{-1}, was kindly received through the Bank of Crystallizable Polymers of European funded COST Action P12 [19]. After drying under vacuum at 100 °C for 16 h, the sample chips were compression-molded with a Carver Laboratory Press at a temperature of 280 °C for 3 min, without any applied pressure, to allow complete melting. After this period, a pressure of about 0.5 t was applied for 2 min. Successively the sample was quickly cooled to room temperature by means of cold water circulating in the plates of the press.

DSC and TMDSC measurements were performed with a Perkin-Elmer Differential Scanning Calorimeter DSC7. The instrument was calibrated in temperature with high purity standards (indium, naphthalene and cyclohexane) according to the procedure for standard DSC. The heat-flow rate was initially calibrated with the heat of fusion of indium, then refined with a run of two empty aluminum pans, and a calibration run with sapphire as a standard for both DSC and TMDSC experiments [20]. Dry nitrogen was used as purge gas at a rate of 30 ml min^{-1}. The sample mass was kept small, approximately equal to 4 mg, to reduce as much as possible the problems that may arise from thermal gradients inside the sample, especially during non-isothermal crystallization [21]. A fresh sample was employed for each analysis in order to minimize thermal degradation.

For DSC runs the following test procedure was used: each compression-molded PET sample was heated from room temperature to 280 °C at a rate of 30 °C min^{-1}, maintained at this

temperature for 3 min, then cooled to 40 °C at various scanning rates, ranging from 2 to 20 °C min^{-1}. Each experimental curve shown below is the average of at least four repeated runs.

TMDSC analyses were designed using the dynamic temperature program that is obtained through a sawtooth modulation in the Perkin-Elmer DSC7. Measurements were conducted using a temperature amplitude (A_T) of 1.0 °C, the chosen modulation period (p) was 60 s, and the underlying cooling rates were 2 and 3 °C min^{-1}. Higher cooling rates are not used with the TMDSC technique because the results would be extremely approximated.

3. Results

3.1. DSC and TMDSC measurements

To determine the kinetics of vitrification of the rigid amorphous fraction during growth of the crystal phase with the here proposed enthalpy-based procedure, it is necessary to obtain quantitative calorimetric data. Fig. 1 shows the influence of cooling rate on the specific heat capacity of PET during cooling from the melt.

As expected, with increasing the cooling rate (q), the crystallization curves shift to lower temperatures: at lower cooling rates there is more time to overcome the nucleation barrier, so crystallization starts at higher temperatures, whereas at higher rates nuclei become active at lower temperatures [22]. The exothermic peaks are quite sharp and steep at the beginning of the phase transition, especially at the lowest cooling rates, which reveals the presence of a large number of active nuclei. Then, at temperatures lower than the peak position, these exotherms become smoother with a long tail that gradually approaches the baseline heat capacity. For the analyzed range of cooling rates, the crystallization process extends from about 230 to 125 °C. At lower temperatures, the c_p step at the glass transition overlap for all the curves, proving that, under the chosen experimental conditions, the amount of mobile amorphous phase that remains after crystallization and possible vitrification of the rigid amorphous fraction is independent of cooling rate. The glass transition, centered at 85 °C, extends from about 100 °C to almost 65 °C, where the specific heat capacity approaches the baseline c_p of the solid polymer. The mobile amorphous fraction at 100 °C, calculated as the ratio between the c_p step of the sample and the c_p step of a fully amorphous sample [6], which is obtained from the ATHAS $c_{p,A}$ and $c_{p,C}$ data, is equal to 0.37.

From the data of Fig. 1, the evolution of crystal fraction was calculated using the classical enthalpy-based procedure summarized in Eq. (2), neglecting, as a first approximation, a possible vitrification of the rigid amorphous fraction [15,16]. Results exhibited in Fig. 2 range from the onset of crystallization to 100 °C, i.e. to immediately above the glass transition temperature of the mobile amorphous phase. As expected, cooling rate affects not only the starting temperature of crystallization, but also the maximum value of crystallinity, which diminishes with increasing the cooling rate [2,22]. Most important is the shape of the curves, all showing a maximum around 150 °C: the apparent crystal fraction seems to increase from the onset of crystallization to reach a maximum, then continuously decreases as T_g is approached.

Since no latent heat seems to be exchanged in the temperature range from 125 to 100 °C (Fig. 1), some errors seem to occur in data processing of Fig. 2, causing a decrease in crystallinity with decreasing temperature. As will be detailed in the next section, this discrepancy is due to vitrification of the rigid amorphous phase [16], which is ignored in the calculations based on Eq. (2).

To confirm the absence of crystallization on cooling in the temperature range from 125 to 100 °C, TMDSC experiments were performed at the underlying cooling rates of 2 and 3 °C min^{-1}. According to the mathematical treatment of TMDSC data, the modulated temperature and the heat-flow-rate curves can be approximated to a Fourier series and separated into an underlying component, approximately equal to the con-

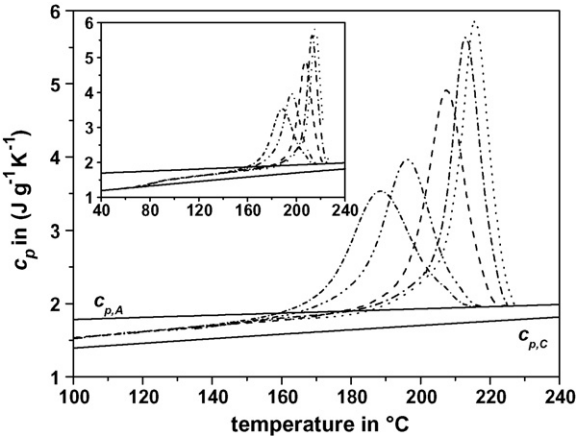

Fig. 1. Specific heat capacity of PET in the crystallization region on cooling at different rates (−20 °C min^{-1}: short dash dot line; −10 °C min^{-1}: dash dot dot line; −5 °C min^{-1}: dash line; −3 °C min^{-1}: dash dot line; −2 °C min^{-1}: dot line) as a function of temperature. The solid lines are the crystalline and mobile amorphous specific heat capacities, as available from ATHAS data bank [17]. In the insert the entire curves down to 40 °C are shown.

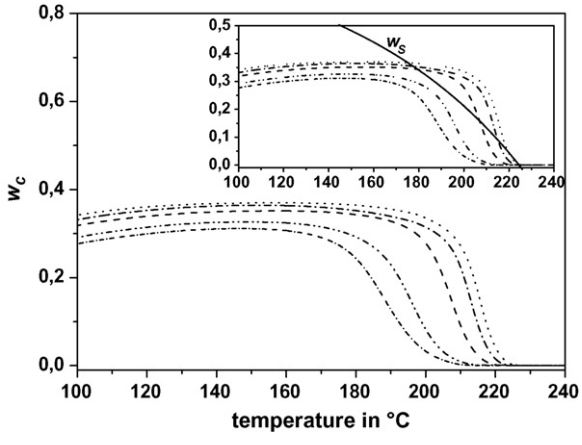

Fig. 2. Crystalline weight fraction (w_C) from the enthalpy-based two-phase method [15,16] on cooling at different rates (−20 °C min^{-1}: short dash dot line; −10 °C min^{-1}: dash dot dot line; −5 °C min^{-1}: dash line; −3 °C min^{-1}: dash dot line; −2 °C min^{-1}: dot line) as a function of temperature. In the insert the solid weight fraction (w_S) curve, calculated by Eq. (20) using the extrapolated linear baseline c_p from the cooling rates 2 and 3 °C min^{-1}, is overlaid (see text).

ventional DSC curves at the same underlying scanning rate, and a periodic component [23,24]. From the periodic components the reversing specific heat capacity can be calculated:

$$c_{\mathrm{p,rev}}(\omega, n, t) = \frac{A_{\Phi,n}(t)}{mn\omega A_{\mathrm{T},n}(t)} \quad (5)$$

where ω is the base frequency of temperature modulation, n the order of the harmonic, $A_{\Phi,n}(t)$ and $A_{\mathrm{T},n}(t)$ the amplitudes of the harmonics of the periodic heat-flow-rate and temperature modulation respectively and m the mass of the sample. As well known, $c_{\mathrm{p,rev}}$ gives information about the processes that can be 'reversed' by temperature modulation. Since the sawtooth temperature profile consists only of odd harmonics, the fact that the even harmonics of the heat-flow-rate response were found practically equal to zero in the whole temperature range covered by the modulated scans was an indication that deviations from linearity and stationarity were negligible and $c_{\mathrm{p,rev}}$ was well described by the ratio of the first harmonics of the heat-flow-rate and temperature [25].

The reversing specific heat capacities, measured at the underlying cooling rates of 2 and 3 °C min^{-1} and found nearly identical, are compared in Fig. 3 with the corresponding data obtained by conventional calorimetry. Starting from the melt, the $c_{\mathrm{p,rev}}$ curves show a peak at about 210 °C, which is considerably less intense than the crystallization peaks obtained from standard DSC. From approximately 170 °C the $c_{\mathrm{p,rev}}$ trend becomes linear down to the glass temperature.

In absence of reversing crystallization/melting processes, the effect evidenced by a TMDSC scan during crystallization is generally the change of the specific heat capacity, which evolves from the melt value towards lower values characteristic of a sample of higher crystallinity and possibly higher rigid amorphous phase content [4]. Thus the reversing specific heat capacity corresponds to the baseline specific heat capacity ($c_{\mathrm{p,base}}$), i.e. the specific heat capacity without contributions from latent heats. Actually, even if crystallization and melting of linear macromolecules are largely irreversible events, a small percentage of reversing crystallization/melting processes can be found in some polymers also during crystallization, that generally is conducted in conditions of supercooling [5,8,26]. Since both the development and absorption of latent heat produce an increase in the modulation amplitude of the heat-flow-rate, independently of the direction of the heat exchanged, the reversing specific heat capacity cannot discriminate between exothermic and endothermic processes occurring during the temperature modulation. More detailed information can be gained from the modulated heat-flow-rate profiles.

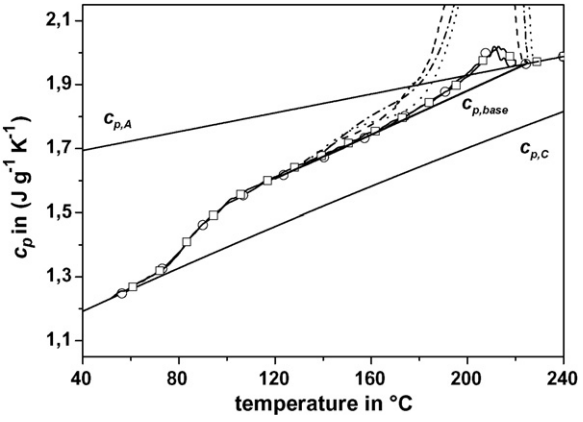

Fig. 3. Specific heat capacity of PET in the crystallization region on cooling at different rates (−5 °C min^{-1}: dash line; −3 °C min^{-1}: dash dot line; −2 °C min^{-1}: dot line) and reversing specific heat capacity (−2 °C min^{-1}: –□–; −3 °C min^{-1}: –◯–) as a function of temperature. The solid lines $c_{\mathrm{p,base}}$, $c_{\mathrm{p,A}}$ and $c_{\mathrm{p,C}}$ are the extrapolated baseline (see text) and the crystalline and the amorphous specific heat capacities respectively, as available from ATHAS data bank [17].

Fig. 4 shows the modulated heat-flow-rate curve obtained at the underlying scanning rate of −2 °C min^{-1} together with its periodic component in different temperature ranges. In the temperature interval 220–210 °C exothermic and maybe also small endothermic effects can be observed in the cooling and heating semiperiods. On the contrary, in the temperature range 170–154 °C no distorsions of the modulated signal appear in both the semicycles, with the periodic heat-flow-rate curve assuming perfectly the shape of a rectangular function. The same observation can be done down to 100 °C. As a result (i) the small peak in the $c_{\mathrm{p,rev}}$ curve, extending from 220 to approximately 170 °C, originates from changes in crystallization rate occurring in the two semiperiods and, perhaps, a reversing crystallization/melting process induced by temperature modulation and (ii) the measured reversing specific heat capacity in the temperature range 170–100 °C corresponds to the baseline specific heat capacity ($c_{\mathrm{p,base}}$).

Moreover, from the comparison with Fig. 1, it can be clarified that the crystallization process starts in the range 230–215 °C (depending on the cooling rate) and extends down to approximately 125 °C. In the temperature range $125 > T > 100$ °C crystallization does not occur on cooling, because the experimental c_{p} from DSC runs is equal to the reversing specific heat capacity from TMDSC scans, both corresponding to the baseline specific heat capacity.

The crystallization data presented in Figs. 1 and 3 were used to determine the kinetics of evolution of the three nanophases of PET during cooling, as detailed below.

3.2. Enthalpy-based method for the determination of crystalline, mobile amorphous and rigid amorphous fraction contents

The experimental enthalpy value, $h(T)$, can be expressed in terms of $h_{\mathrm{C}}(T)$, $h_{\mathrm{A}}(T)$ and $h_{\mathrm{RA}}(T)$ which represent specific enthalpy values of crystalline, mobile amorphous and rigid amorphous fractions, respectively:

$$h(T) = w_{\mathrm{C}}(T)h_{\mathrm{C}}(T) + w_{\mathrm{A}}(T)h_{\mathrm{A}}(T) + w_{\mathrm{RA}}(T)h_{\mathrm{RA}}(T) \quad (6)$$

Being $w_{\mathrm{C}}(T) + w_{\mathrm{A}}(T) + w_{\mathrm{RA}}(T) = 1$, Eq. (6) can be rewritten as:

$$w_{\mathrm{C}}(T) = \frac{h_{\mathrm{A}}(T) - h(T)}{h_{\mathrm{A}}(T) - h_{\mathrm{C}}(T)} + w_{\mathrm{RA}}(T)\frac{h_{\mathrm{RA}}(T) - h_{\mathrm{A}}(T)}{h_{\mathrm{A}}(T) - h_{\mathrm{C}}(T)} \quad (7)$$

from which it results that the crystalline weight fraction for a three-phase model is given by the value calculated for the

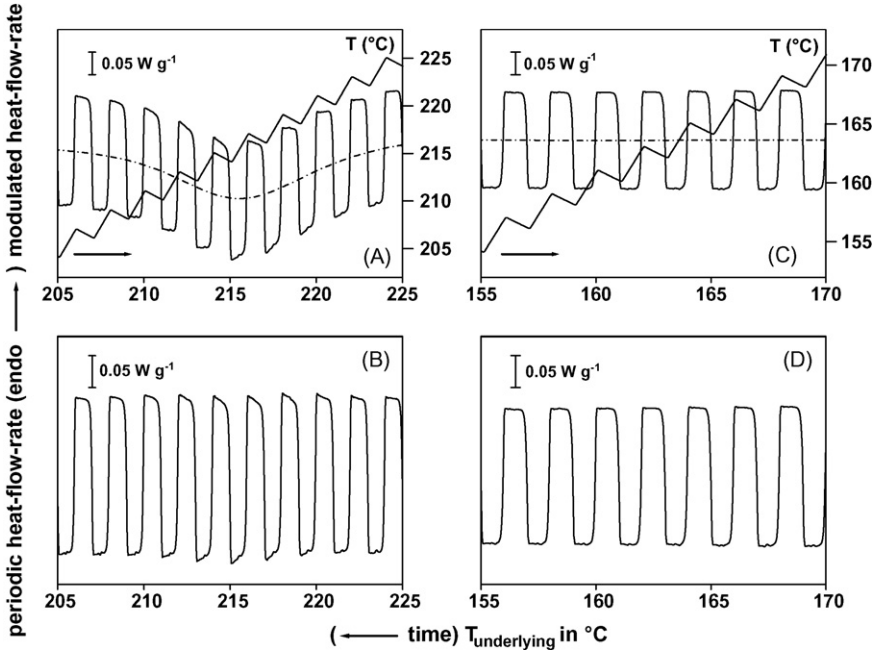

Fig. 4. TMDSC data obtained with the following operative conditions: period = 60 s, temperature modulation amplitude = 1.0 °C, underlying cooling rate = 2 °C min^{-1}. (A) Modulated and underlying heat-flow-rate curves (solid and dashed lines, respectively) in the temperature range 225–205 °C as a function of the underlying temperature. The modulation temperature profile, referred to the right *Y*-axis, is also shown. (B) Periodic heat-flow-rate curve in the temperature range 225–205 °C. (C) Modulated and underlying heat-flow-rate curves (solid and dashed lines, respectively) in the temperature range 170–155 °C. (D) Periodic heat-flow-rate curve in the temperature range 170–155 °C.

two-phase model (see Eq. (3)) plus a term related to both the content and the specific enthalpy of the rigid amorphous fraction.

From the fundamental relationship (6) the specific heat capacity for a three-phase system can be obtained:

$$c_p(T) = \frac{dh(T)}{dT} = w_C(T)c_{p,C}(T) + w_A(T)c_{p,A}(T) + h_C(T)\frac{dw_C(T)}{dT} + h_A(T)\frac{dw_A(T)}{dT} + \frac{d[w_{RA}(T)h_{RA}(T)]}{dT} \quad (8)$$

where the derivative of the product $w_{RA}(T)h_{RA}(T)$ has to be defined.

Certainly the enthalpy of the rigid amorphous phase is connected to the thermal history of the sample, since, at each temperature, it is the weighted sum of the enthalpy of the RAF that is produced at that temperature and the enthalpy of the RAF formed previously at higher temperatures during the cooling run. The enthalpy of the RAF that solidifies at a given temperature T is equal to the enthalpy of the mobile amorphous fraction at that temperature, as prescribed by thermodynamics for the glass transition [27]. As regards the enthalpy of the RAF formed at higher temperatures, its temperature derivative is known by assuming, with good approximation, that the heat capacity of the glassy material is equal to that of the crystal phase, being both considered as solid fractions [6,16,28].

Therefore, according to the definition of derivative:

$$\frac{d[w_{RA}(T)h_{RA}(T)]}{dT} = \lim_{\Delta T\to 0}\frac{w_{RA}(T+\Delta T)h_{RA}(T+\Delta T) - w_{RA}(T)h_{RA}(T)}{\Delta T} \quad (9)$$

and by setting

$$w_{RA}(T+\Delta T) = w_{RA}(T) + \Delta w_{RA} \quad (10)$$

and

$$h_{RA}(T+\Delta T) = \frac{w_{RA}(T)[h_{RA}(T) + c_{p,C}(T)\Delta T] + \Delta w_{RA}h_A(T+\Delta T)}{w_{RA}(T) + \Delta w_{RA}} \quad (11)$$

it can be obtained:

$$\frac{d[w_{RA}(T)h_{RA}(T)]}{dT} = \lim_{\Delta T\to 0}\frac{w_{RA}(T)c_{p,C}(T)\Delta T + \Delta w_{RA}h_A(T+\Delta T)}{\Delta T} \quad (12)$$

that becomes:

$$\frac{d[w_{RA}(T)h_{RA}(T)]}{dT} = w_{RA}(T)c_{p,C}(T) + h_A(T)\frac{dw_{RA}}{dT} \quad (13)$$

Thus, by substituting this result in Eq. (8), it is demonstrated that the specific heat capacity of a three-phase system that accounts for the crystalline, mobile amorphous phase and rigid

amorphous phases respectively, is described by the following equation:

$$c_p(T) = w_C(T)c_{p,C}(T) + w_A(T)c_{p,A}(T) + w_{RA}(T)c_{p,C}(T) - [h_A(T) - h_C(T)]\frac{dw_C(T)}{dT} \quad (14)$$

Eq. (14) has already been reported in the literature, even if obtained with a different mathematical treatment [16].

Being defined the two fundamental relationships for a three-phase system (Eqs. (6) and (14), respectively), an expression to calculate $h_{RA}(T)$ can be attained starting from the temperature dependence of the experimental enthalpy $h(T)$:

$$h(T) = h(T_1) + \int_{T_1}^{T} c_p(T)\,dT' \quad (15)$$

where T_1 is a reference temperature in the melt ($T_1 > T$), at which no RAF is present, so that $h(T_1) = h_A(T_1)$, and c_p the experimental specific heat capacity expressed by Eq. (14).

The substitution of Eq. (14) in Eq. (15), after integration by parts of the term $[h_A(T) - h_C(T)]\,dw_C(T)$, yields:

$$h(T) = w_C(T)h_C(T) + [1 - w_C(T)]h_A(T) + \int_{T_1}^{T} w_{RA}(T)[c_{p,C}(T) - c_{p,A}(T)]\,dT' \quad (16)$$

By equalling Eqs. (6)–(16), the following final expression is obtained:

$$h_{RA}(T) - h_A(T) = \frac{1}{w_{RA}(T)}\int_{T_1}^{T} w_{RA}(T)[c_{p,C}(T) - c_{p,A}(T)]\,dT' \quad (17)$$

from which the difference between the enthalpies of the rigid amorphous and the mobile amorphous fractions can be determined once the $w_{RA}(T)$ function is known.

Lastly, Eq. (7) can be rewritten by substituting the term $[h_{RA}(T) - h_A(T)]$ and introducing the solid weight fraction $w_S(T) = w_C(T) + w_{RA}(T)$, to yield:

$$w_C(T) = \frac{h_A(T) - h(T)}{h_A(T) - h_C(T)} + \frac{\int_{T_1}^{T}[w_S(T) - w_C(T)][c_{p,C}(T) - c_{p,A}(T)]\,dT'}{h_A(T) - h_C(T)} \quad (18)$$

Eq. (18) is a relationship of fundamental importance since it permits to obtain the crystalline weight fraction for a three-phase system with a successive approximations method if the total solid content $w_S(T)$ is known. This latter can be gained from the baseline specific heat capacity. In fact, in absence of latent heat contributions, the baseline c_p can be expressed from Eq. (14) as:

$$c_{p,base}(T) = w_C(T)c_{p,C}(T) + w_A(T)c_{p,A}(T) + w_{RA}(T)c_{p,C}(T) \quad (19)$$

Proper reorganization of Eq. (19) yields:

$$w_A(T) = \frac{c_{p,base}(T) - c_{p,C}(T)}{c_{p,A}(T) - c_{p,C}(T)} \quad (20)$$

Being $w_S(T) = [1 - w_A(T)]$, Eq. (20) easily allows to determine the mobile amorphous and the solid fractions respectively starting from the baseline c_p.

A last observation can be added about the baseline specific heat capacity. Since its derivative with respect to temperature is given by:

$$\frac{dc_{p,base}(T)}{dT} = w_A(T)\frac{dc_{p,A}(T)}{dT} + [w_C(T) + w_{RA}(T)]\frac{dc_{p,C}(T)}{dT} + [c_{p,A}(T) - c_{p,C}(T)]\frac{dw_A(T)}{dT} \quad (21)$$

it comes out that the slope of $c_{p,base}(T)$ is intermediate between the slopes of $c_{p,A}(T)$ and $c_{p,C}(T)$ only if the weight fractions of all the phases are constant. If not, an additional term has to be considered.

For the cooling rates 2 and 3 °C min^{-1}, the baseline c_p, which is known only in the temperature range 170 > T > 100 °C (Fig. 1), as a first approximation can be extrapolated up to the melt by following the same linear trend displayed from 100 to 170 °C (Fig. 3). Moreover, it can be hypothesized that the baseline c_p at 2 and 3 °C min^{-1} also holds for the cooling rate 5 °C min^{-1}. The $w_S(T)$ curve calculated from the linear baseline c_p is depicted in the insert of Fig. 2 together with the $w_C(T)$ curves from the two-phase model (Eq. (3)) for all the cooling rates investigated. The intersection of the $w_C(T)$ curves at 2, 3 and 5 °C min^{-1} with the $w_S(T)$ curve occurs at temperatures slightly and progressively higher than 170 °C (see Table 1).

A hypothesis can be formulated according to which the polymeric system PET cooled at 2, 3 and 5 °C min^{-1} has to be described by a three-phase and two-phase model at temperatures, respectively, lower and higher than the intersection point of Fig. 2. In other words in a PET sample cooled at 2, 3 and 5 °C min^{-1}, the rigid amorphous fraction would develop at temperatures lower than 180 °C, i.e. during the final stages of the crystallization process. This finding is in perfect agreement with results from heating and cooling scans reported in ref. [29] according to which RAF in PET disappears between 160 and 180 °C, depending on the thermal history of the sample. Elsewhere it has been proposed that RAF could be glassy up to about 220 °C, but the hypothesis has not been undoubtedly confirmed [10]. The fact that in Fig. 2 the $w_C(T)$ curves for the cooling rates 10 and 20 °C min^{-1} do not intersect the w_S curve should be due to a different baseline $c_p(T)$.

Since the mobile amorphous fraction $w_A(T)$, and therefore $w_S(T)$, can be calculated without approximations in the temperature range from 100 to 170 °C, that is to approximately the intersection points of Fig. 2, the crystalline weight fraction $w_C(T)$ for a three-phase system can be calculated by means of Eq. (18) in this interval with a successive approximations procedure, using as initial value the crystalline weight fraction from the two-phase method, calculated from Eq. (3). The successive approximations method is reiterated until no further change of

Table 1
Cooling rate dependence of (i) $w_C(T) - w_S(T)$ curves intersection points and (ii) maximum values of the crystalline weight fraction from the two-phase ($w_{C,max}$) and the three-phase models (w_C^0)

Cooling rate (°C min^{-1})	Intersection point of $w_C(T) - w_S(T)$ curves in °C from Fig. 2	$w_{C,max}$, two-phase model from Eq. (3)	w_C^0, three-phase model from Eq. (18)
2	175.2	0.37o	0.37$_9$
3	177.5	0.36$_4$	0.37o
5	179.5	0.35$_2$	0.36$_2$
10	–	0.326	–
20	–	0.31$_2$	–

The small digits are non-significant figures.

$w_C(T)$ is obtained. After determination of the crystalline weight fraction, the RAF content can be obtained by difference. It is worth noting that Eq. (18) can be applied only in the temperature range in which the baseline c_p is available, as the knowledge of the correct $w_A(T)$, and as consequence $w_S(T)$, is indispensable for the calculation of $w_C(T)$. The fact that $w_{RA}(T)$ is achieved by difference from $w_A(T)$ and $w_C(T)$ does not allow to operate with also the baseline $c_p(T)$ as variable function subjected to successive approximations, since at the end of each iterative cycle, the $c_{p,base}(T)$ calculated by Eq. (19) would come out unchanged.

In order to link the crystalline fractions from the two-phase and three-phase models respectively, a linear extrapolation of the baseline heat capacity, that is found linear from 100 to 170 °C, is performed in a very narrow temperature range beyond 170 °C up to the intersection points reported in Table 1. The extrapolation interval is so small, that minor uncertainty about the determination of the temperature at which the rigid amorphous phase starts to develop is expected.

Fig. 5 shows the $w_C(T)$, $w_A(T)$ and $w_{RA}(T)$ curves in the whole crystallization range for the cooling rates 2, 3 and 5 °C min^{-1}, respectively. From the melt down to the intersection points of Fig. 2, $w_C(T)$ and $w_A(T)$ are from the two-phase method (Eq. (3)) whereas at lower temperatures the three-phase method (Eq. (18)) is applied. The presence of cusps in the $w_A(T)$ and $w_{RA}(T)$ curves is due to the sharp mathematical switch from one model to the other and to the incomplete accuracy of the linear extrapolation of $c_{p,base}(T)$ from 170 °C up to the intersection points. Smoother curves are certainly more probable, even if not predictable *a priori*.

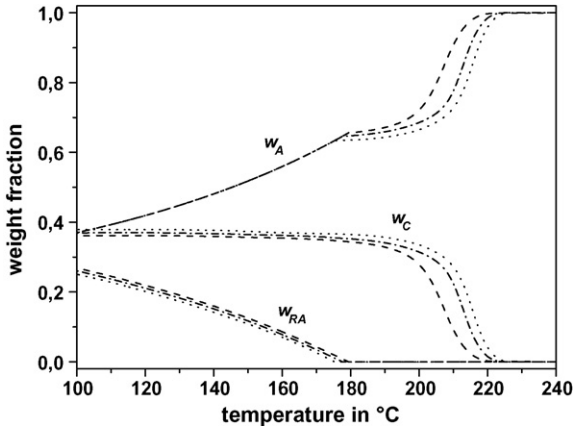

Fig. 5. Crystalline weight fraction (w_C), mobile amorphous weight fraction (w_A) and rigid amorphous weight fraction (w_{RA}) as a function of temperature (−5 °C min^{-1}: dash line; −3 °C min^{-1}: dash dot line; −2 °C min^{-1}: dot line). The curves in the temperature range between 100 °C and the intersection points of Fig. 2 are from the enthalpy-based three- phase method (see text), those in the temperature range between the intersection points and 240 °C from the enthalpy-based two-phase method [15,16].

As expected, cooling rate affects the final value of crystallinity, which diminishes with increasing the cooling rate. The mobile amorphous fraction decreases with decreasing temperature whereas the rigid amorphous fraction has an opposite trend. Moreover in the temperature range $180 > T > 100$ °C $w_{RA}(T)$ depends on the cooling rate: as expected, lower contents of rigid amorphous phase are found after crystallization at the lowest cooling rates. In fact it has already been reported that RAF content is higher under crystallization conditions that promote formation of imperfect crystallites [30]. In addition, it is worth noting that the average rigid fraction content calculated at 100 °C (approximately equal to 0.25) is identical to the value reported in ref. [6] for PET samples crystallized at different temperatures.

The comparison between the crystalline fraction from the three-phase and the two-phase models is shown in Fig. 6 for the cooling rate 3 °C min^{-1}.

The decrease of the two-phase $w_C(T)$ observed as the temperature lowers towards the glass transition is ascribable to the formation of RAF that reduces the baseline c_p and consequently the term $[h_A(T) - h(T)]$ in Eq. (3), calculated by integration of the c_p curves (see also ref. [16]). The concomitant increase of the experimental enthalpy value $h(T)$ with respect to the case in

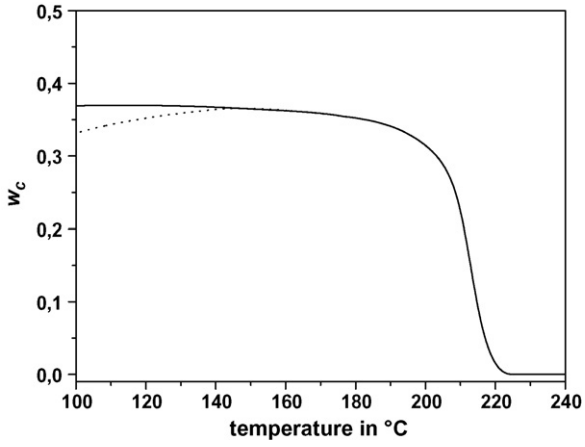

Fig. 6. Comparison between the crystalline weight fraction (w_C) from the enthalpy-based two-phase method (dash line) [15,16] and the enthalpy-based three-phase method (solid line) (see text) for the cooling rate 3 °C min^{-1}.

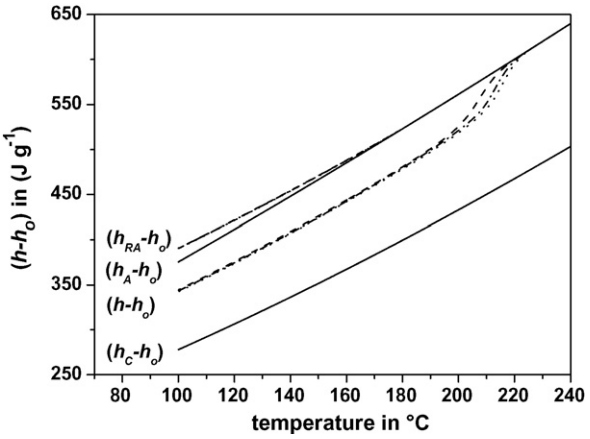

Fig. 7. Temperature dependence of the crystalline ($h_C - h_0$), experimental ($h - h_0$), mobile amorphous ($h_A - h_0$), and rigid amorphous ($h_{RA} - h_0$) enthalpies for the cooling rates 2, 3 and 5 °C min^{-1}. The crystalline and mobile amorphous enthalpies are from ATHAS data bank [17] the rigid amorphous and experimental enthalpies are from Eqs. (22) and (23), respectively.

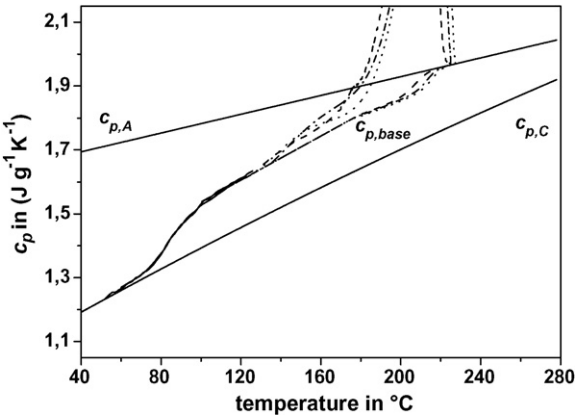

Fig. 8. Specific heat capacity of PET in the crystallization region on cooling at different rates and the relative baseline specific heat capacity $c_{p,base}(T)$, calculated from Eq. (19) (−5 °C min^{-1}: dash line; −3 °C min^{-1}: dash dot line; −2 °C min^{-1}: dot line).

which RAF is not produced has not to be ascribed to an improbable fusion process, as could appear from the two-phase $w_C(T)$ trend, but arises from the higher enthalpic content of the RAF.

In fact, being the function $w_{RA}(T)$ accessible in the whole crystallization range for the cooling rates 2, 3 and 5 °C min^{-1}, the specific enthalpy of the rigid amorphous phase produced under these experimental conditions can be calculated via Eqs. (17) and (22):

$$[h_{RA}(T) - h_0] = [h_{RA}(T) - h_A(T)] + [h_A(T) - h_0] \quad (22)$$

where h_0 is the unknown enthalpy of the crystal at 0 K, at which all the enthalpy values are referred and $[h_A(T) - h_0]$ the tabulated mobile amorphous fraction [17].

Also the experimental enthalpy, i.e. $[h(T) - h_0]$ can be obtained starting from the measured $[h_A(T) - h(T)]$ curves:

$$[h(T) - h_0] = [h_A(T) - h_0] - [h_A(T) - h] \quad (23)$$

The temperature dependence of $[h_{RA}(T) - h_0]$, $[h(T) - h_0]$, $[h_A(T) - h_0]$, and $[h_C(T) - h_0]$ can be shown in Fig. 7 for the cooling rates 2, 3 and 5 °C min^{-1}.

A significant aspect that immediately comes out is that the specific enthalpy of the rigid amorphous phase results higher than that of the mobile amorphous phase, converging towards it in proximity of the temperature at which RAF starts to develop (see also arguments provided in ref. [16]). For the cooling rates analyzed, the curves $[h_{RA}(T) - h_0]$ almost overlap each other, indicating that the slightly different experimental conditions affect very little the enthalpic content of the RAF. Moreover, a regular trend with the cooling rate is found for the curves $[h(T) - h_0]$, with a little lower enthalpic contents showed by the samples which, cooled at the lowest rates, are characterized by a higher crystalline fraction.

As final result, Fig. 8 reports the baseline specific heat capacity, $c_{p,base}(T)$, calculated according to Eq. (19) for the cooling rates 2, 3 and 5 °C min^{-1} with the data from Fig. 5. As expected, the baseline specific heat capacity shows a sigmoid shape in correspondence of the crystallization peak.

4. Discussion

It has already pointed out that the most striking feature of the $w_C(T)$ *versus* T plots shown in Fig. 2, calculated with the classical procedure based on a two-phase model, is the shape of the curves, all showing a maximum followed by a continuous decrease until the onset of the glass transition is reached. This trend might be explained paradoxically with the occurrence of partial fusion of the already crystallized material, but neither the DSC nor the TMDSC curves display any evidence of this impossible endothermic event. This suggests that some errors occurred in the data processing that led to the curves of Fig. 2. An obvious source of error may be found in the possible vitrification of amorphous chains at temperatures higher than T_g, a process that could overlap or immediately follow crystallization and that has been ignored in the calculations based on Eq. (2).

However the crystallinity values of PET at the end of crystallization at 2, 3 and 5 °C min^{-1} from the three-phase model (w_C^0) are only slightly higher than the crystalline values exhibited at the maximum of the curves in Fig. 2 ($w_{C,max}$) (see in Table 1 and the example given in Fig. 6). Such similarity is due to the fact that vitrification of the rigid amorphous fraction in PET starts during the final stages of the crystallization process, so that from the beginning of the crystallization down to about 180 °C the two-phase model is valid for PET cooled at 2, 3 and 5 °C min^{-1}.

The three-phase method here proposed allows to determine the temperature at which vitrification of the rigid amorphous phase begins and the kinetics of the process by taking into account the change of the baseline c_p during crystallization. This change, as described above, is due to both the growth of the crystal phase and the vitrification of the rigid amorphous phase. Quantitative separation of the irreversible latent heat effects from the diminution of baseline c_p due to solidification can be gained from TMDSC curves. Reversing c_p data taken from Fig. 3 allow to know the temperature variation of the baseline specific heat capacity. When cooling is conducted at rates of 2 and 3 °C min^{-1}, the temperature dependence of the baseline c_p is

not accessible in the whole crystallization temperature range, but only in the interval $170 > T > 100\,^{\circ}C$, as discussed above. Therefore in principle the crystalline and rigid amorphous fractions contents could not be attained by means of the enthalpy-based method here proposed because the integral of Eq. (18) has to be calculated starting from the melt temperature. Luckily it has been demonstrated that for PET cooled at 2, 3 and $5\,^{\circ}C\,min^{-1}$ the classical two-phase model can be applied correctly in the temperature range in which the baseline c_p is not available, so that the $w_C(T)$, $w_A(T)$ and $w_{RA}(T)$ curves can be calculated in the whole solidification interval.

If the baseline c_p is totally indefinite in the whole temperature range in which crystallization occurs, an estimation of the final crystalline weight fraction can be constituted by $w_{C,max}$ from the two-phase model (Table 1). In the temperature range in which the crystallization process is completed, the constant crystalline weight fraction can be set equal to $w_{C,max}$ and the approximate $w_A(T)$ and $w_{RA}(T)$ curves can be determined from Eq. (20) and by difference, respectively. The results of this procedure applied to PET in the temperature interval $125 > T > 100\,^{\circ}C$ are illustrated in Fig. 9 for all the cooling rates investigated. As expected lower contents of rigid amorphous phase are found after crystallization at the lowest cooling rates.

The experimental results here reported reveal that the kinetics of vitrification of the RAF in poly(ethylene terephthalate) is only partially linked to the crystallization process. The rigid amorphous structure starts to vitrify during the final stages of the non-isothermal crystallization, with the full establishment of the rigid amorphous structure completed during the subsequent cooling to room temperature, in excellent agreement with results reported in ref. [10]. The possibility of parallel development of crystalline and rigid amorphous phases has been analyzed up-to-date for a few polymers. For poly(3-hydroxybutyrate) (PHB), bisphenol-A polycarbonate (PC) and isotactic polystyrene (iPS) a simultaneous increase of the crystal phase and solidification of the RAF was found during cold crystallization (PHB, iPS) and melt crystallization (PC) [7–9]. This led to the conclusion that for these polymers vitrification of the RAF results from the morphological changes associated to the crystallization process. In these cases it is probable that the presence of rigid amorphous phase limit further growth of the crystals. On the contrary, similarly to PET, in syndiotactic polypropylene (sPP) RAF was found to vitrify partly together with the growth of the crystal phase during cold crystallization and partly upon cooling in a temperature range of about 40 °C [7,8]. Hence, for PET as for sPP, the limitation of crystal growth due to vitrification of the surrounding melt material could be excluded.

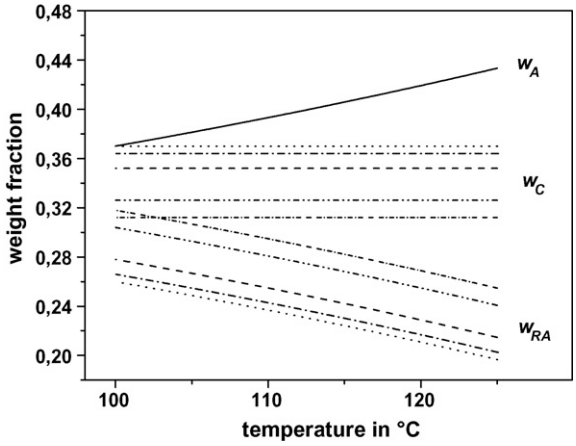

Fig. 9. Approximate crystalline weight fraction (w_C), mobile amorphous weight fraction (w_A) and rigid amorphous weight fraction (w_{RA}) in the temperature range $125 > T > 100\,^{\circ}C$ (see text) ($-20\,^{\circ}C\,min^{-1}$: short dash dot line; $-10\,^{\circ}C\,min^{-1}$: dash dot dot line; $-5\,^{\circ}C\,min^{-1}$: dash line; $-3\,^{\circ}C\,min^{-1}$: dash dot line; $-2\,^{\circ}C\,min^{-1}$: dot line).

As shown in Figs. 1 and 3, melt crystallization exotherms in PET displays a smooth tail at low temperatures, probably due to slow secondary crystallization. In effect the three-phase enthalpy-based $w_C(T)$ reported in Fig. 5 for the cooling rates 2, 3 and $5\,^{\circ}C\,min^{-1}$ are found to increase slightly with decreasing temperature in the range $180 > T > 100\,^{\circ}C$, suggesting that crystallization, almost finished at 180 °C, continues slowly through a secondary crystallization process after spherulite impingement [2].

Up to now, the exact mechanism of secondary crystallization in PET has not been totally clarified yet. During a cooling it should involve only further growth of crystallites more defective, being the perfection process through thickening of the lamellae unlikely under such operative conditions [2]. A few different models have been proposed, including the insertion of thin lamellae into the interlamellar region and/or the insertion of thin lamellar stacks between the stacks of lamellar crystals formed in the primary crystallization [31]. Despite the ongoing debates, some correlation of vitrification of the amorphous phase with secondary crystallization seems acceptable, being the interlamellar amorphous layers often claimed as the most likely "geographical" locations for RAF [32]. It is likely that before spherulite impingement the polymer chains have a sufficiently high mobility so that not large constraints are imposed on the amorphous phase. Once spherulite impingement has occurred, further crystallization can take place only in geometrically restricted areas, where the amorphous fraction experiences larger constraints, which in turn results in vitrification of the rigid amorphous phase [9,32,33].

As regards the temperature dependence of the enthalpy of the rigid amorphous phase, calculated by Eq. (17) and shown in Fig. 7, it is important to point out that this finding is a significant experimental proof of the theoretical hypotheses formulated in refs. [6,16]. The enthalpy of the rigid amorphous phase results higher than that of the mobile amorphous phase due to a higher free volume [34] and/or energy content of the constrained system. It is well known that during vitrification the free volume freezes as a consequence of severe restriction in the macromolecular segmental mobility, so that at each temperature the volume of the RAF results higher than that of the corresponding MAF.

5. Conclusions

The enthalpy-based determination of crystal and amorphous fractions that relies on a two-phase description of semicrys-

talline polymers is often applied also in the presence of a rigid amorphous fraction [4,5]. The errors so produced can be minor when a small amount of rigid amorphous phase is present, or relevant for polymers where a large fraction of amorphous phase is solid above T_g. To avoid these errors, Eqs. (2)–(4) should be applied only above the glass transition of the RAF, but this requires an *a priori* estimation of the temperature range of devitrification of the RAF, which is usually not known.

For a limited group of semicrystalline polymers this information is available, like poly(oxy-2,6-dimethyl-1,4-phenylene), whose RAF has a glass transition above the melting point [12] or poly(butylene terephthalate), where the T_g of the RAF is centered around 102 °C and extends over a range of ca. 70 °C [28]. However, the exact locations of vitrification and devitrification of the rigid amorphous structure are generally not directly identifiable from DSC curves because, unlike the main transitions involving the mobile amorphous phase and the crystal phase, formation and disappearance of the RAF are generally associated to the continuous changes of structure of crystal and mobile amorphous phases occurring during or after partial crystallization and fusion [7–9].

The enthalpy-based three-phase method here presented has been used to determine the kinetics of crystallization and vitrification of the RAF in PET during non-isothermal solidification processes. The rigid amorphous fraction was found to develop partly during the final stages of the crystallization process and partly during cooling down to T_g.

The results shown seem to confirm the existence of a link between vitrification of the rigid amorphous phase and secondary crystallization in PET.

By comparing data from various polymers, as detailed above [7–10] it is evident that different polymers and different crystallization paths affect the amount of RAF produced simultaneously to crystallization. Although some similarities exist, each polymer, due to its particular molecular structure, has specific peculiarities in the primary and secondary crystallizability as well as in the connected vitrification of the rigid amorphous phase.

Acknowledgements

The authors wish to thank the Bank of Crystallizable Polymers of European funded COST Action P12 for kindly providing the PET sample. M.L.D.L. gratefully acknowledges the financial support received by Italian Ministero dell'Istruzione dell'Università e della Ricerca (MIUR), D.D. 9-10-02, prot. n. 1105/2002.

References

[1] B. Wunderlich, Macromolecular Physics. Crystal Structure, Morphology Defects, vol. 1, Academic Press, New York, 1973.
[2] B. Wunderlich, Macromolecular Physics. Crystal Nucleation, Growth Annealing, vol. 2, Academic Press, New York, 1976.
[3] B. Wunderlich, Macromolecular Physics. Crystal Melting, vol. 3, Academic Press, New York, 1990.
[4] B. Wunderlich, Thermal Analysis of Polymeric Materials, Springer-Verlag, New York, 2005.
[5] B. Wunderlich, Progr. Polym. Sci. 28 (2003) 383–450.
[6] M. Alsleben, C. Schick, Thermochim. Acta 238 (1994) 203–207.
[7] C. Schick, A. Wurm, A. Mohammed, Colloid Polym. Sci. 279 (2001) 800–806.
[8] C. Schick, A. Wurm, A. Mohammed, Thermochim. Acta 396 (2003) 119–132.
[9] H. Xu, S. Ince, P. Cebe, J. Polym. Sci,. Part B: Polym. Phys. 41 (2003) 3026–3036.
[10] R. Androsch, B. Wunderlich, Polymer 46 (2005) 12556–12566.
[11] A.A. Minakov, D.A. Mordvintsev, R. Tol, C. Schick, Thermochim. Acta 442 (2006) 25–30.
[12] J. Pak, M. Pyda, B. Wunderlich, Macromolecules 36 (2003) 495–499.
[13] R. Rastogi, W.P. Weling, S. Rastogi, C. Schick, H.E.H. Meijer, J. Polym. Sci.: Part B: Polym. Phys. 42 (2004) 2092–2106.
[14] M.C. Righetti, M.L. Di Lorenzo, M. Angiuli, E. Tombari, Macromolecules 37 (2004) 9027–9033.
[15] V.B.F. Mathot, R.L. Scherrenberg, M.F.J. Pijpers, W. Bras, J. Thermal Anal. 46 (1996) 681–718.
[16] V.B.F. Mathot, in: V.B.F. Mathot (Ed.), Calorimetry and Thermal Analysis of Polymers, Hanser/Gardner, Cincinnati, 1994, pp. 105–167.
[17] ATHAS Data Bank, M. Pyda (Ed.), Web address: http://www.prz.rzeszow.pl/athas/databank/intro.html.
[18] M.L. Di Lorenzo, M. Pyda, B. Wunderlich, J. Polymer Sci., Part B: Polym. Phys. 39 (2001) 1594–1604.
[19] COST P12 ACTION, web site: http://www.uni-rostock.de/fakult/manafak/physik/poly/COST_P12/index.htm.
[20] D.G. Archer, J. Phys. Chem. Ref. Data 22 (1993) 1441–1453.
[21] M.L. Di Lorenzo, S. Cimmino, C. Silvestre, Macromolecules 33 (2000) 3828–3832.
[22] M.L. Di Lorenzo, C. Silvestre, Prog. Polym. Sci. 24 (1999) 917–950.
[23] A. Boller, Y. Jin, B. Wunderlich, J. Thermal Anal. 42 (1994) 307–330.
[24] J.E.K. Schawe, E. Bergman, W. Winter, J. Thermal Anal. 54 (1998) 565–576.
[25] M. Merzlyakov, C. Schick, J. Thermal. Anal. Calorim. 61 (2000) 649–659.
[26] B. Goderis, H. Reynaers, R. Scherrenberg, V.B.F. Mathot, M.H.J. Kock, Macromolecules 34 (2001) 1779–1787.
[27] G.B. McKenna, in: G. Allen, J.C. Bevington (Eds.), Comprehensive Polymer Science, vol. 2, Pergamon, London, 1988, pp. 311–362.
[28] M. Pyda, E. Nowak-Pyda, J. Heeg, H. Huth, A.A. Minakov, M.L. Di Lorenzo, C. Schick, B. Wunderlich, J. Polym. Sci. Part B: Polym. Phys. 44 (2006) 1364–1377.
[29] I. Okazaki, B. Wunderlich, Macromolecules 30 (1997) 1758–1764.
[30] S.X. Lu, P. Cebe, Polymer 37 (1996) 4857–4863.
[31] R. Verma, H. Marand, B. Hsiao, Macromolecules 29 (1996) 7767–7775.
[32] B.B. Sauer, B.S. Hsiao, Polymer 36 (1995) 2553–2558.
[33] H. Lu, P. Cebe, Macromolecules 37 (2004) 2797–2806.
[34] J. Lin, S. Shenogin, S. Nazarenko, Polymer 43 (2002) 4733–4743.